Journal of Statistical Mechanics: Theory and Experiment
An IOP and SISSA journal

Experimental study of a creeping granular flow at very low velocity

Jérôme Crassous, Jean-François Metayer, Patrick Richard and Claude Laroche

Institut de Physique de Rennes, UMR CNRS 6251, Université Rennes 1, 263 av. Général Leclerc, 35042 Rennes Cedex, France
E-mail: jerome.crassous@univ-rennes1.fr, jean-francois.metayer@univ-rennes1.fr, patrick.richard@univ-rennes1.fr and claude.laroche@hotmail.fr

Received 4 December 2007
Accepted 18 February 2008
Published 13 March 2008

Online at stacks.iop.org/JSTAT/2008/P03009
doi:10.1088/1742-5468/2008/03/P03009

Abstract. We report an experimental study of the surface flow and the creeping flow of glass spheres on a heap. We characterize the dynamics of the flow with particle tracking velocimetry and dynamic light scattering measurements. We observe a creeping flow with a dynamics which slows down exponentially with the depth. The characteristic distance for the decay is one bead diameter. A striking observation is that the exponential decay for the mean velocity holds over more than six orders of magnitude.

Keywords: granular matter, heterogeneous materials (experiment)

J. Stat. Mech. (2008) P03009

Contents

1. Introduction

Surface flows of granular materials are a common case of granular flow in which only a shallow layer of particles flows on a fixed bed of the same particles [1]. Such flows may occur in many different practical situations, such as the transport of sediment in rivers or flows on a heap. Although a considerable effort has been made in order to understand them [1], the behavior of such flows is far from being fully understood. At a first look at a surface flow, we may distinguish a rapidly flowing phase moving on a static bed of granular material. However, a more careful investigation shows that the bed is not strictly static, but also flows with a mean velocity which may be several orders of magnitude smaller than the surface flow. The comprehension of such 'creeping flow', and its connection with the surface flow, are still debated topics. We propose in this paper to have a look at the mean velocity profile of the creeping flow under a heap of glass spheres. The velocity profile is measured with two complementary techniques. For the surface flow and the relatively rapid creeping flow, the mean velocity is extracted from particle tacking velocimetry measurements. More deeply under the surface, we used a dynamic light scattering measurement which gives access to the shear rate. With the combination of the two techniques, we were able to measure the variations of the velocity over nine orders of magnitude.

doi:10.1088/1742-5468/2008/03/P03009

J. Stat. Mech. (2008) P03009

In section 2 we recall different experimental results on the measurement of creeping flow. In section 3, we describe our experimental set-up. The experimental results are discussed in section 4. The analysis of the experimental data of dynamic light scattering is given in section 5. Finally, in section 6 we report the velocity profiles as measured with the two complementary techniques.

2. Creeping flows

The aim of the present experimental work is to obtain information on creeping flow. For this, we will combine two complementary techniques, particle tracking velocimetry, and dynamic light scattering. Before dealing with the details of the experiments, we first recall some published experimental results on creeping flows. The pioneering work on creeping flow below surface flow is due to Komatsu *et al* [2]. They studied the creeping flow of millimetric spheres, sand and seed flowing on a two-dimensional hopper. The velocity profiles for different flow rates and particles types were obtained by snapshots of the pile with different shutter speeds. The mean velocity profiles were found to vary quite linearly with the depth in a rapidly flowing zone, and the thickness of the flowing zone was found to depend on the flows rate, from 5 to 15 diameters d of particles in the experiment. Under the rapidly flowing zone, the velocity decays exponentially with the depth, with a characteristic length ξ independent of the flows rate, and ranging from $\approx$1.35 diameters for spheres, to $\approx$0.6 diameters for sand. Taberlet *et al* [3] also observed the same kind of creeping flow below the rapidly flowing zone for glass spheres flowing on a superstable granular heap, but did not report an analysis of the velocity decay. The same kind of creeping flow was also reported in rotating drum geometry. Bonamy *et al* [4] reported an experiment on the flow of steel beads of diameter d in a rotating drum at low Froude number. They measured the velocity profile for steady surface flows with particle tracking velocimetry, and distinguished a flowing layer and a 'static phase' where creeping motion takes place. The velocity decay inside the static phase was found to decay exponentially, with a characteristic decay $\xi \approx 2.5d$. They also noticed that neither this characteristic length nor the velocity gradient depends on the drum rotating velocity, the effect of velocity being only an increase of the thickness of the flowing layer. Socie *et al* [6] reported experiments on painted millimetric spherical glass spheres in a rotating drum, and reported similar behavior with an exponential decay of the velocity with a characteristic decay $\xi \approx 3.4d$. Orphe *et al* [7] reported an experiment on the steady flow of millimetric steel and brass spheres in a rotating drum. They reported also a linear velocity profile and a creeping zone with an exponential decay of the mean velocity, with a characteristic decay $\xi = 1.1 \pm 0.2d$. They also measured the variation of the root mean square (rms) velocity in the same zone, and showed that the fluctuations also decay exponentially, with a characteristic length $\xi_{\mathrm{rms}} = 1.7 \pm 0.3d$. Courrech du Pont *et al* [8] reported on the velocity profiles during avalanches of millimetric spherical glass beads in a rotating drum experiment. They showed that also in unsteady flows, the creeping flows decay exponentially, with a characteristic length $\xi = 3 \pm 1d$. Finally, Mueth *et al* [9] reported an experiment on the flow of spherical and non-spherical seeds in a cylindrical Couette geometry. They measured the dependence of the mean azimuthal velocity with respect to the radial distance. They show that the mean velocity decays over a typical distance which was of the order of the diameter of a grain. A noticeable difference from

J. Stat. Mech. (2008) P03009

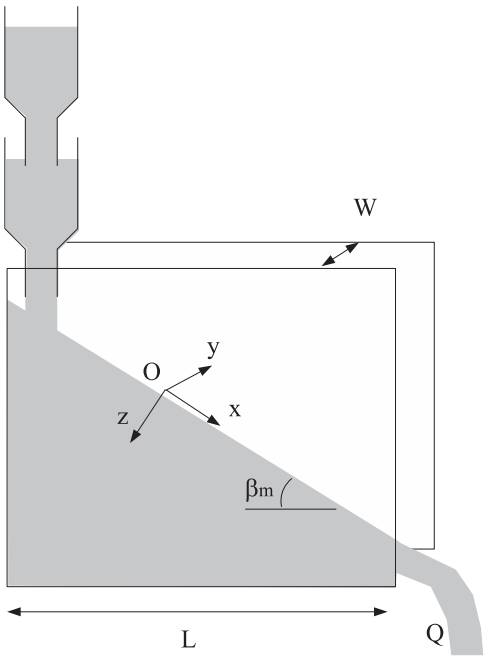

Figure 1. The heap geometry with the coordinate system and the parameters.

the other reported experiments is that the decay law appears to be a Gaussian law. This difference has been attributed to the geometry of the experiment [2]. All the results are summarized in table 1.

3. Experiments

3.1. Flow geometry

The heap geometry that we studied is schematically shown in figure 1. It is a super stable heap [10] between two parallel plates. The plates are square and their size L is 400 mm. They are made of 6 mm thick floated glass and are separated with the use of spacers of a width $W = 5$ mm.

We study the flow of spherical soda-lime glass beads from 'Marteau & Lemarié' company. The experiments reported here were done with beads of diameter d in the range 0.4–0.6 mm. Small dust was removed by sieving. We will use the mean value $d = 0.5$ mm for the following discussions. Observations of the beads with a microscope show that a few per cent of the beads are broken beads or have a shape which is clearly elliptical. Experiments not presented here have been also performed with beads of mean diameters $d = 0.2$ mm and $d = 0.3$ mm with very similar results for the velocity profiles measured both with particle tracking velocimetry and dynamic light scattering. However, possibly due to the drift of hygrometry and the important presence of dust particles despite careful sieving, the results are not fully reproducible over time. Moreover, small beads have a slight tendency to segregate at the interface between the rapid flow and the creeping flow. Since dynamic light scattering must be averaged over a time relatively long compared to the time during which segregation seems to occurs, this may introduce a

J. Stat. Mech. (2008) P03009

Table 1. Summary of some experiments on creeping flows. d is the diameter for spherical particles.

Authors	Geometry	Material	Velocity range (m s^{-1})	Decay length/ diameter ξ/d
Komatsu [2]	Heap	Alumina spheres, sand, seed	10^{-2}–10^{-6}	1
Bonamy [4]	Rotating drum	Steel beads	10^{-1}–10^{-3}	2.5
Jain [5]	Rotating drum	Steel and glass spheres	10^{-1}–10^{-3}	$1-2$
Socie [6]	Rotating drum	Painted spherical glass	10^{-2}–10^{-4}	4.9
Orpe [7]	Rotating drum	Steel and brass spheres	10^{-1}–10^{-2}	1.1 ± 0.2
Courrech du Pont [8]	Rotating drum (non-stationary)	Glass spheres	10^{-1}–10^{-3}	3 ± 1
Mueth [9]	Couette cell	Seed	10^{-1}–10^{-4}	Gaussian decay
This work	Heap	Glass spheres	10^{-2}–10^{-9}	1 ± 0.2

systematic error. The flow of granular material is driven continuously at a constant flow rate Q with a system of a double funnel. We present here an experiment with a flow rate $Q = 30 \pm 1$ g s^{-1}, and the results are similar for a smaller rate. After a few seconds of transient regime, the mean slope β_m of the heap attains a constant value $\beta_m = 45 \pm 2°$ and the flow appears stationary.

3.2. Particle tracking velocimetry

The velocities in the rapid flow zone and in the beginning of the creeping zone are measured with the analysis of images of the flow. For this, the flow is lit with a white spot and specular reflections are imaged with a fast camera Photron APX RS at a resolution of 1024×1024 pixels and at frame rates of 100 00, 1500 and 50 image s^{-1} and with a Nikon D200 camera with a resolution 3872×2592 pixels and a frame rate of 0.2 image s^{-1}. The beads have a size of about 30 pixels and their trajectories are defined using a tracking program. The only beads that can be tracked are the one close to the sidewalls. The computation of the velocity vectors requires first processing images in order to improve the quality, then determining the center of the beads. Velocities are then computed as the difference between the positions of the beads between successive images. In order to obtain the mean velocity, we average the velocity of the grains of a slice of a thickness $\Delta z = 0.35$ mm and of length $\Delta x = 22$ mm, and on a sequence of a few thousand images. Variations of the intensity of the light source produce small variations in the gray level of each pixel. This noise limits the precision of our measurement, i.e. the smallest displacement that can be detected. In order to determine this precision, the positions of grains in an immobile sample are tracked. The displacements measured are then considered to be displacement artifacts due to spot light variations. We then estimate that the minimum average velocity that we can detect is $\approx 1/(200\delta t)$ mm s^{-1}, where δt is the interval in seconds between two successive images.

J. Stat. Mech. (2008) P03009

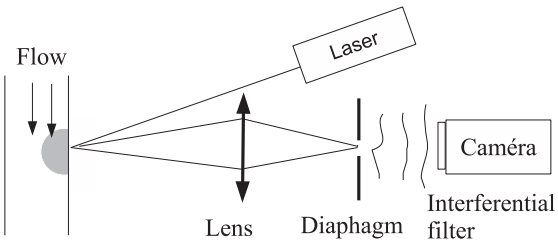

Figure 2. Schematic drawing of the dynamic light scattering set-up.

3.3. Dynamic light scattering

The dynamics of the creeping flow is also investigated with a dynamic light scattering experiment. A sketch of the experiment is shown in figure 2. The granular medium is illuminated with a laser (Quantum Coherent, vacuum wavelength $\lambda_0 = 0.532$ μm). The light is then scattered, and the image of the surface is projected on an iris diaphragm. The scattered light is then collected with a Panasonic camera which acquires images at a frame rate of 20 image s^{-1}. The size of the speckle spot is typically 3 pixels. Because experimental data need to be averaged over a long experimental run, we only acquire $N = 2456$ pixels on the camera. It has been checked that restricting the acquisition to such a number of pixels does not introduce a significant noise on the estimate of the correlation function of the scattered intensity. The scattered intensity $I(t, p)$, where t is the acquisition time and p is the index of the pixel, is then measured. The normalized correlation function of the scattered light is defined as [12, 11]

$$g_I(\tau) = \frac{\langle I(t,p)I(t+\tau,p)\rangle_{t,p}}{\langle I(t,p)\rangle_{t,p}\langle I(t,p)\rangle_{t+\tau,p}} - 1 \tag{1}$$

where τ is the lag time and $\langle\cdot\rangle_{t,p}$ means an average over the times t and the acquired pixels p. For an accurate determination of (1) the correlation of the dark noise of the camera has been subtracted following a procedure given elsewhere [13]. The total acquisition time for each experiment is 20 min, and the first three minutes of every acquisition have been dropped in order to be in a stationary state. Indeed, it appears that deeply in the flow, a typical time of one minute is needed in order to obtain stationary dynamics. The minimum lag time is fixed by the frame rate, i.e. 50 ms. The maximum attainable lag time is fixed by the coherence of the laser. In order to estimate this time, we measured the temporal correlation of the light scattered by a granular medium at rest. From this measurement, we estimate that the decorrelation due to laser fluctuation is not relevant if the lag time is smaller than $\sim$60 s.

For practical reasons, the velocities and the dynamic light scattering are measured roughly 10 cm before the exit of the heap. The flow seems well established and stationary everywhere, expect in the first and the last centimeter of the heap. The origin for the vertical axis $z = 0$ is arbitrarily located and marked. This origin is the same for the particle tracking velocimetry and the light scattering experiments. In practice, this origin coincides roughly with the maximum of the ballistic trajectories of the grains.

J. Stat. Mech. (2008) P03009

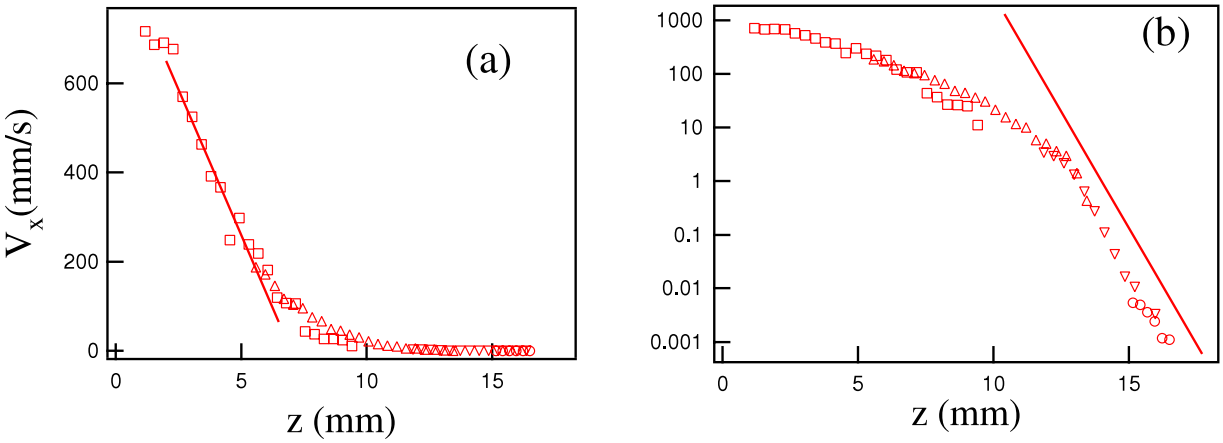

Figure 3. Mean velocity profile determined from particle tracking velocimetry measurements. Symbols are experimental measurements at different acquisition rates □: 100 00 i/s, △ : 1500 i/s, ▽: 50 i/s and ○: 0.2 i/s. (a) is a linear plot. The line corresponds to a constant shear rate $\dot{\gamma}_a = 130\ \mathrm{s}^{-1}$. (b) is a logarithmic plot. The solid line is a exponential decay $V_x \propto \exp(-z/\xi)$ with a characteristic length $\xi = 1.1d$.

4. Experimental results

4.1. Particle tracking velocimetry

The velocity of the flowing layer and in the creeping flow determined from the particle tracking velocimetry is plotted on figure 3. The velocities of the grains in the top layers between $z = 0$ and 1 mm are not measured. In this zone, the motions of the grains are clearly ballistic, and difficult to obtain with our particle tracking parameters. As shown in figure 3(a), in the dense flow zone, the velocity is first quite constant and decays roughly linearly up to $z/d \approx 14$, and then decreases more slowly. Such velocity profiles are very typical of what is commonly measured for dense surface flow [7, 10]. We define an average shear rate $\dot{\gamma}_a$ as the mean slope of the curve V_x versus z in the region where the variations of the velocity V_x with the depth z are linear. We estimate $\dot{\gamma}_a = 130 \pm 10\ \mathrm{s}^{-1}$. This value may be compared with the measurement of Orpe *et al* [7]. Those authors show that the shear rate is related to the slope of the surface according to the phenomenological equation [14]

$$\dot{\gamma}_c = \left[\frac{g\sin(\beta_\mathrm{m} - \beta_s)}{cd\cos(\beta_s)}\right]^{1/2} \tag{2}$$

where g is the acceleration due to gravity, β_m is the mean slope of the heap, β_s the repose angle of the heap, and c is a numerical constant of order unity. Taking $\beta_\mathrm{m} = 45°$, $\beta_s = 24°$, and $c = 0.56$ [7] leads to $\dot{\gamma}_a = 117\ \mathrm{s}^{-1}$, in reasonable agreement with our observation.

We observe in figure 3(b) that, at smaller velocity, a very different behavior occurs. The velocity decays exponentially as

$$V_x \propto \exp(-z/\xi) \tag{3}$$

J. Stat. Mech. (2008) P03009

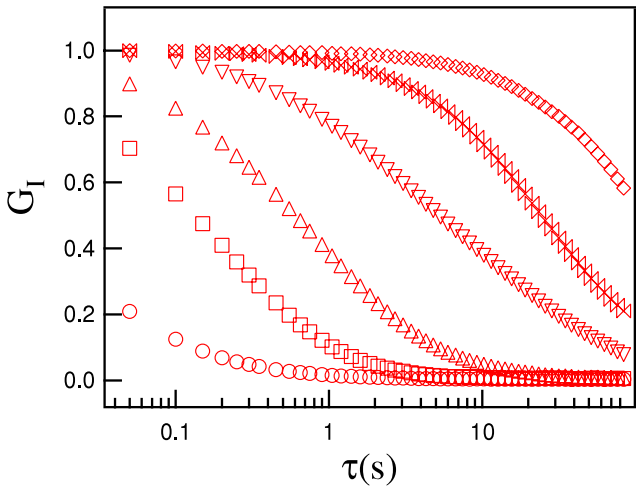

Figure 4. Normalized correlation function of the scattered intensity as a function of the lag time τ. Different symbols correspond to different experiments performed at different depths z: (○) 16 mm, (□) 17 mm, (△) 18 mm, (▽) 19 mm, (⋈) 20 mm and (◇) 21 mm.

with the characteristic length for this exponential decay being $\xi = 1.0 \pm 0.1d$. The decay law for the velocity as a function of the depth, and the value of the characteristic decay ξ, are in agreement with the previously reported studies recalled in section 2.

4.2. Dynamic light scattering

Figure 4 shows the correlation functions of the scattered intensity G_I. They are measured for different depths ranging between 16 and 21 mm below the free surfaces. The typical error on the localization of the laser spot with respect to the mark indicating the $z = 0$ level is roughly ≈0.3 mm. Different experiments have been performed on different days with the same flow rate in order to check the reproducibility of the results. For every experiment, the correlation decays smoothly with the lag time τ. The rate of the relaxation depends strongly on the depth, and the dynamics is slowed down by four orders of magnitude between the extreme measurements separated in depth by a distance of 5 mm.

The different curves representing the correlation functions collapse on a master curve if the lag time is rescaled by a characteristic time τ_0. We take arbitrary $\tau_0 = 1$ s for experiments performed at $z = 18$ mm. The figure 5 shows the effect of this scaling. The variation of the characteristic time τ_0 as a function of the depth z is plotted in the inset of figure 5. The variation of the characteristic time τ_0 is found to follow an exponential law over the full range of experimental data:

$$\tau_0 \propto \exp(z/\xi') \tag{4}$$

where $\xi' = 1.1 \pm 0.1d$ is the characteristic length for the slowing down of the dynamics. The decay of the dynamics of the light scattering data occurs with the same exponential law and the same characteristic length as the decay of the velocity measured with particle tracking velocimetry higher in the flow. This strongly suggests that dynamic light scattering data could be interpreted with the hypothesis that the mean velocity of

J. Stat. Mech. (2008) P03009

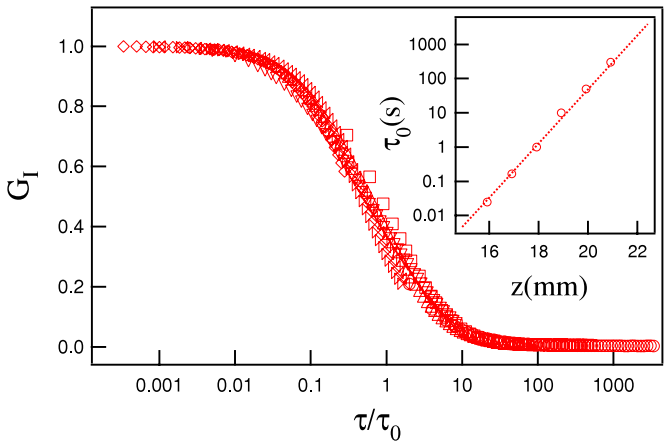

Figure 5. Normalized correlation function of the scattered intensity as a function of the rescaled lag time τ/τ_0. The symbols are the same as for figure 4. Inset: variation of the time τ_0 as a function of the depth. The dotted line is an exponential fit $\tau_0 \propto \exp z/\xi'$ with $\xi' = 1.1d$.

the grains decays with the same exponential law over the full range of depth within the creeping flow.

5. Modeling of dynamic light scattering data

5.1. Dynamic light scattering and shear flow

The relationship between the dynamics of particles within a disordered medium and the fluctuations of the scattered light is a very classical problem which has been addressed in various experimental configurations. The dynamics of the multiple scattered light of colloidal particles submitted to a stationary shear flow has been investigated by different authors [20]–[23]. The results have been extended to the shearing of emulsions [15] and to the deformations of a granular medium [25]. In dynamic light scattering experiments, when the scattered electric fields are Gaussian distributed, the intensity correlation function is related to the intensity autocorrelation function by the Siegert relation [16]:

$$g_I(\tau) = 1 + |g_E(\tau)|^2 \tag{5}$$

where $g_E(\tau) = \langle E(t)E^*(t+\tau)\rangle / \langle |E(t)|\rangle^2$ is the correlation function of the scattered electric field E. Within the weak scattering limit ($kl \gg 1$, where k is the wavenumber, and l the scattering mean free path), and in the multiply scattering limit ($L \gg l$, L being the typical size of the cell), the intensity of the light can be described by the diffusion approximation [17]. The autocorrelation function is then given by [18, 19]

$$g_E(\tau) = \int P(s)\langle \exp[j\Delta\phi_s(\tau)]\rangle \mathrm{d}s \tag{6}$$

where $P(s)$ is the fraction of the total scattered intensity which is scattered in a path of length s. $\Delta\phi_s(\tau)$ is the phase difference of the electric field between time t and time $t+\tau$ associated with a given multiple scattering path of length s, and information about the

J. Stat. Mech. (2008) P03009

dynamics of the system is contained in this quantity. The average $\langle\cdot\rangle$ in (6) represents an average over all possible paths of all possible orientations for a photon propagating in the sample. It can be shown [20]–[23] that for a stationary shear flow the average of the fluctuation of phase variation $\langle\exp[j\Delta\phi_s(\tau)]\rangle$ may be expressed as

$$\langle\exp[j\Delta\phi_s(\tau)]\rangle = \exp[-2(s/l^*)(\tau/\tau_s)^2] \tag{7}$$

where l^* is the transport mean free path. The characteristic time for the decay is

$$\tau_s = \frac{\sqrt{30}}{k_0 l^* \dot{\Gamma}} \tag{8}$$

where $k_0 = 2\pi/\lambda_0$ and $\dot{\Gamma}$ is a combination of the component of the strain rate tensor $e_{ij}^2 = (1/2)(\partial_i V_j + \partial_j V_i)$:

$$\dot{\Gamma} = \sqrt{2\sum_{i,j}\overline{e_{ij}^2}}. \tag{9}$$

In (9), $\overline{e_{ij}^2}$ represents an average of e_{ij}^2 over the local density of photons inside the sample. This simply says that the more a zone in the sample is lit, the more important is its contribution to the scattered field [20]–[22].

The meaning of (7)–(9) may be easily understood. The decorrelation of the scattered electric field or intensity depends on the variation of the length of the optical paths, and those variations come from the deformations of the material. The decays of the correlation functions for sheared colloidal particles [21]–[23] and emulsions [15] are found to be in agreement with (7)–(9).

In this description, the decay of the autocorrelation function is only sensitive to the deformation of the material, and not to a translation without deformation. However, a single translation of the granular material will induce a translation of the speckle pattern, and then a loss of correlation of the scattered light. If we consider a translation of the granular material at a velocity V, the speckle pattern moves at the same velocity. With a speckle spot size l_c, we may expect a loss of correlation on a timescale $\tau_t \approx l_c/V$. Taking $\dot{\Gamma} \sim V/\xi$ with $\xi \sim 500$ μm, $l^* \sim 1.2$ mm (see section 5.2), $l_c \approx 3$ pixels ≈ 40 μm, we obtain $\tau_s/\tau_t \sim 5 \times 10^{-3}$. So translation without deformation induces a loss of correlation on a timescale at least two orders of magnitude larger than the decorrelation induced by the shearing of the granular material.

5.2. Constant shear rate modeling

In the preceding expressions (7)–(9), the characteristic time τ_s varies as the inverse of the average strain rate $\dot{\Gamma}$, and then as the inverse of the velocity field components V_i. It follows that if all the components of the velocity field are divided by an arbitrary factor λ, the characteristic time τ_s is multiplied by a factor λ, and hence the characteristic timescales for the variations of g_E and g_I. So, the exponential variations of τ_0 given by (4) may be interpreted if we assume that the component of the velocity field decreases with depth as

$$V_i \propto \exp(-z/\xi') \tag{10}$$

where $\xi' = 1.1 \pm 0.1d$.

J. Stat. Mech. (2008) P03009

It should be stressed that this result does not depend on a particular choice for the distribution function $P(s)$ of the optical path length.

It follows from the comparison between (3) and (10) and from the comparison between the values for the characteristic length ξ and ξ' that light scattering data may be interpreted with the assumption that the velocity field varies as

$$V_x(x, y, z) = V_0 \exp(-z/\xi'). \tag{11}$$

Expression (11) is surely a crude description of the velocity field. First, the velocity is expected to depend on the distance from the glass plates. Indeed it has been shown numerically [3] and experimentally [8] that the velocity field inside the gap is close to a plug flow, with a variation $\partial_y V_x \sim d/6$ near the surfaces. However, those variations are negligible compared to $\partial_x V_x \sim d$ in the estimate of the mean strain rate $\dot{\Gamma}$ given by (9). Other effects that are not taken into account in (11) are possible fluctuations of the mean velocities or rotations of the beads if they are not strictly spherical. If such motions are present, they should induce fluctuations on the path lengths, and then participate in the loss of correlation of the scattered intensity.

With the simple velocity field given by (11), we have

$$\dot{\Gamma} \simeq \frac{V_o}{\xi'} \exp(-z/\xi'). \tag{12}$$

In the derivation of (12), we suppose that the strain rate tensor components $\overline{e_{ij}^2}$ are constant everywhere on the lit zone. We will relax this hypothesis later. The distribution of path length $P(s)$ depends on the geometry for the illumination. In the backscattering geometry on a half space, the path distribution $P(s)$ may be calculated and then g_E and g_I (5) [24]:

$$g_I(\tau) \simeq \left| \exp\left(-\gamma \sqrt{\tfrac{1}{5}} k_0 l^* \dot{\Gamma} \tau \right) \right|^2 \tag{13}$$

where $\gamma \simeq 2.0$ is a numerical factor.

The correlation function corresponding to (13) is calculated and compared to experimental data in figure 6. We used the value $l^* = 1.22 \pm 0.24$ mm that we obtained from measurements of the optical transmissivity of the beads. The value for the mean stain rate $\dot{\Gamma}$ simply shifts the timescale on a logarithmic plot. We represent (13) for a mean strain rate $\dot{\Gamma} = 2.2 \times 10^{-4}/\tau_0$. Although the form of the variation is in rough agreement with experimental observations, equation (13) shows a decrease sharper than the experimental variations. The main limitation of this simple model is easy to understand. The extension of the zone from which the light is backscattered is of the order of $l^* \approx 2d$. There are then photons which explore zones where the mean strain rate is lower or greater than the average mean strain rate. It follows that we expect a broad distribution of the timescales for the decay of the correlation function and then a stretching of the decay compared to a simple exponential decay. Moreover, the geometry for our experiment is a slab of granular material and not an half plane. This should presumably change the distribution of path length $P(s)$ and then the functional form for g_I compared to a simple exponential decay.

J. Stat. Mech. (2008) P03009

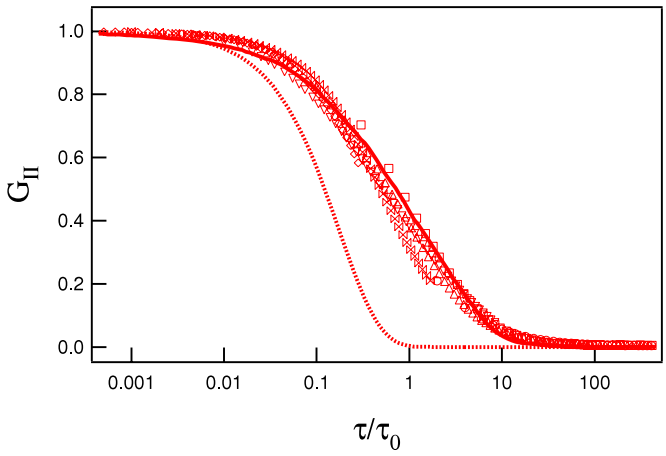

Figure 6. Normalized correlation function of the scattered intensity as a function of the rescaled lag time τ/τ_0. The symbols are the same as for figure 4. Dotted line: correlation function g_I from (13) for a mean strain rate $\dot{\Gamma} = 2.2 \times 10^{-4}/\tau_0$. Plain line: correlation function g_I obtained from the ray tracing model with an exponentially varying strain rate, the mean strain rate being $\dot{\Gamma} = 2.2 \times 10^{-4}/\tau_0$ at the center of the beam.

5.3. Exponential shear rate

In order to take into account the geometry effects and the non-homogeneous shear in the flow, we need to model more carefully the paths followed by the photons within the granular material. Since the beads are large compared to the laser wavelength, we use the framework of geometrical optics in order to determine the distribution of path length for photons propagating through the glass sphere packing [25]. We first notice that in the geometrical optics approximation, the transport mean free path l^* for a random close packing of monodisperse glass spheres in air is found to be $l^* \approx 3.32d$. For a mean diameter $d = 500$ μm, we then expect $l^* \approx$ 1.66 mm, in reasonable agreement with the measured value $l^* = 1.22 \pm 0.24$ mm. This indicates that treating light propagation with geometrical optics is a quite safe approximation. A plausible explanation for the difference may come from the fact that the granular medium is composed of grains which are neither perfectly spherical nor monodisperse, but we do not take such refinements into account in our model. The correlation function of the scattering electric field $g_E(\tau)$ is then calculated as

$$g_E(\tau) = \frac{\sum_{m=1}^{M} \exp(j\Delta\Phi^{(m)}(\tau)) \exp(-s^{(m)}/l_a)}{\sum_{m=1}^{M} \exp(-s^{(m)}/l_a)}. \tag{14}$$

In (14) the summation is performed over the geometrical rays computed from the geometrical optics ray, m being the number of the ray, and M the total number of rays. $\Delta\Phi^{(m)}(\tau)$ is the phase shift for the ray m with a delay time τ. The length of the ray m is $s^{(m)}$, and the factor $\exp(-s^{(m)}/l_a)$ takes into account absorption into the medium, i.e., large loops into the granular material are more attenuated than short loops. The absorption length may be extracted from transmissivity measurement [26, 27], and we found $l_a = 24 \pm 5$ mm. The phase shift $\Delta\Phi^{(m)}(\tau)$ is calculated from the deformation of

J. Stat. Mech. (2008) P03009

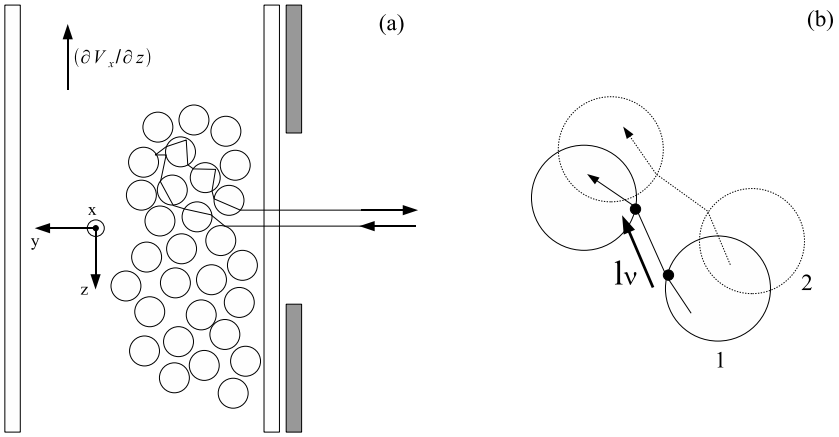

Figure 7. (a) Geometry for the generation of the path for photons in the geometrical optic framework. (b) Schematic drawing of the variation of a segment of the ray when beads are moved from position 1 (plain spheres) to position 2 (dotted spheres).

the segment of the ray which joins spheres. Let $\mathbf{l}^\nu$ be a segment of the ray which joins two spheres as shown in figure 7(b). When the extremities of the ray move with a velocity field $\mathbf{V}(\mathbf{r})$, over a duration τ, the variation of the length l^ν is

$$\Delta l^\nu \simeq \tau \sum_{i,j} \left(\frac{\partial V_i}{\partial x_j} \right) \frac{l_i^\nu l_j^\nu}{l^\nu} \tag{15}$$

where $\sum_{i,j}$ means a summation over x, y, z for i and j. The phase shift is the computed as

$$\Delta\Phi^{(m)}(\tau) = k_0 \sum_\nu \Delta l^\nu \tag{16}$$

where the summation is taken over all segments ν of the ray number m. From (14) to (16), we are able to calculate $g_I(\tau)$ for a velocity field $V_x(x, y, z) = V_0 \exp(-z/\xi')$. The result and comparison to the experimental data are shown as the plain line on (figure 6). The number of rays M for this estimate is $M = 60\,000$, and we take $\xi' = 1.1d$ and the velocity at the center of the beam $V_0 = 2.2 \times 10^{-4}\ \xi'/\tau_0$. The differences with the more simple exponential model given by (13) are quite small. With the same strain rate at the center of the beam, the dynamics is a little bit slower with the optical geometric model compared to the simple exponential decay. This may be understood by the fact that in our slice geometry with absorption the path lengths should be shorter than for an unbounded plane geometry without absorption. The spreading of the timescale for the decay reflects the distribution of strain rate in the lit zone of the creeping flow.

6. Summary of experimental results

The modeling of dynamic light scattering developed in section 5 allows us to have access to the mean velocity. We now compare this determination with the measurement done with the particle tracking velocimetry measurement. Figure 8 is a semi-logarithmic

J. Stat. Mech. (2008) P03009

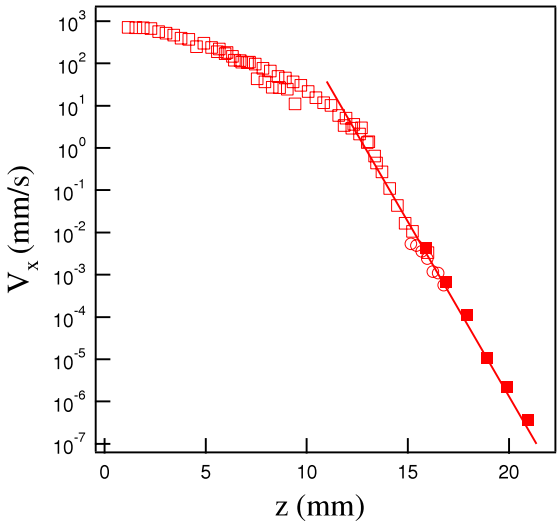

Figure 8. Summary of the measurement of the velocity. Open symbols are velocity measured from particle tracking velocimetry with a fast camera and solid symbols are the velocity determined from dynamic light scattering experiments. The line is an exponential law $V_x \propto \exp(-z/\xi)$ with $\xi = 1.05d$.

plot of the velocity determined by both particle tracking velocimetry and dynamic light scattering. We may clearly see in this figure than the velocities determined with the two different techniques are well matched and overlapped. A careful look at the profiles shows that there is a slight shift of $\approx 0.8d$ between the two exponential velocity profiles, the velocity determined with dynamic light scattering being slightly greater than the velocity determined by particle tracking velocimetry in the zone where they are determined by the two techniques. A possible explanation could be rotational motions of beads or the fluctuating part of the velocity of the beads. Finally we see that the exponential decrease on the velocity field in the creeping flow is indeed verified on the full scale of the measurement, i.e. is valid for 15ξ and more than six decades in velocity.

7. Conclusions

The study of the generic behaviors of granular flows are important for the developments of granular hydrodynamics. The creeping flows which occur below surface flow clearly have a very generic behavior. They occur, as we recalled in section 2, in many different experimental situations. The measure of the fluctuating part of the scattered electric field allows us to obtain information about the motion of the grains at very small velocity. We showed that those experimental observations are in full agreement with the hypothesis of a velocity which decreases exponentially with depth. It is quite fascinating to see that this characteristic decay for the dynamics of the flows persists as long it is possible to measure it. This strongly extends the generality of creeping flow in granular media.

Acknowledgments

We thank Axelle Amon, Christophe Baravian, Renaud Delannay and Sebastien Kriesgen de Richter for fruitful discussions. Hervé Orain and Stephane Bourles helped us with

the mechanical design of the experiments. This work has been supported by ANR grant NT05-4_42012 'MICMAC'.

References

[1] GDR MiDi, 2004 *Eur. Phys. J.* E **14** 341
[2] Komatsu T, Inagaki S, Nakagawa N and Nasuno S, 2001 *Phys. Rev. Lett.* **86** 1757
[3] Taberlet N, *Ecoulements dravitaires de matériaux granulaires*, 2005 *PhD Thesis No 3199* University of Rennes
[4] Bonamy D, Daviaud F and Laurent L, 2002 *Phys. Fluids* **14** 1666
[5] Jain N, Ottino J and Lueptow R, 2002 *Phys. Fluids* **14** 572
[6] Socie B, Umbanhowar P, Lueptow R, Jain N and Ottino J, 2005 *Phys. Rev.* E **71** 031304
[7] Orpe A and Khakhar D, 2007 *J. Fluid. Mech.* **571** 1
[8] Courrech du Pont S, Fisher R, Gondret P, Perrin B and Rabaud M, 2005 *Phys. Rev. Lett.* **94** 048003
[9] Mueth D, Debreageas G, Karczmar G, Eng P, Nagel R and Jaeger H, 2000 *Nature* **406** 385
[10] Taberlet N, Richard P, Valance A, Losert W, Pasini J, Jenkins J and Delannay R, 2003 *Phys. Rev. Lett.* **91** 264301
[11] Viasnoff V, Lequeux F and Pine D, 2002 *Rev. Sci. Instrum.* **73** 2336
[12] Cipelletti L and Weitz D, 1999 *Rev. Sci. Instrum.* **70** 3214
[13] Djaoui L and Crassous J, 2005 *Gran. Mater.* **7** 185
[14] Khakhar D, Orpe A, Andersèn V and Ottino J, 2001 *J. Fluid Mech.* **441** 255
[15] Hebraud P, Lequeux F, Munch J and Pine D, 1997 *Phys. Rev. Lett.* **78** 4657
[16] Berne B and Pecora R, 1976 *Dynamic Light Scattering: With Applications to Chemistry, Biology, and Physics* (New York: Wiley)
[17] Ishimaru A, 1978 *Wave Propagation and Scattering in Random Media* (New York: Academic)
[18] Maret G and Wolf P, 1987 *Z. Phys.* **65** 409
[19] Pine D, Weitz D and Herbolzheimer E, 1990 *J. Physique* **51** 2102
[20] Bicout D, Akkermans E and Maynard R, 1991 *J. Physique* **1** 471
[21] Bicout D and Maynard R, 1993 *Physica* A **199** 387
[22] Bicout D and Maret G, 1994 *Physica* A **210** 87
[23] Wu X, Pine D, Chaikin P, Huang J and Weitz D, 1990 *J. Opt. Soc. Am.* **7** 15
[24] Weitz D and Pine D, 1993 *Dynamic Light Scattering* ed W Brown (Oxford: Clarendon) pp 652–720
[25] Crassous J, 2007 *Eur. Phys. J.* E **23** 145
[26] Li J, Lisyanski A, Cheung T, Livdan D and Genack A, 1993 *Eur. J. Phys.* **22** 675
[27] Leutz W and Rička J, 1996 *Opt. Commun.* **126** 260